

X-Mesh: A new approach for the simulation of two-phase flow with sharp interface

Antoine Quiriny^a, Jonathan Lambrechts^a, Nicolas Moës^{b,c}, Jean-François Remacle^a

^a*Institute of Mechanics, Materials and Civil Engineering (iMMC), Avenue Georges Lemaître 4, 1348 Louvain-la-Neuve, Belgium*

^b*Nantes Université, École Centrale de Nantes, rue de la Noë, 44321 Nantes, France*

^c*Institut Universitaire de France (IUF)*

Abstract

Accurate modeling of moving boundaries and interfaces is a difficulty present in many situations of computational mechanics. We use a new approach, X-Mesh, to simulate with the finite element method the interaction between two immiscible flows while keeping an accurate and sharp description of the interface without remeshing. The surface tension between the two fluids is added thanks to the ghost fluid method which when coupled with X-Mesh allows us to be exactly sharp in the pressure jump. This reduces the parasitic currents due to the surface tension down to the numerical precision.

1. Introduction

The finite element method has been predominant in computational mechanics since the early 1970s. Besides the fact that finite elements are based on a robust mathematical theory [1], a fundamental reason why finite elements are popular is the fact that it can use unstructured meshes that allows accurate discretization of boundaries or interfaces for example between two different materials. When these interfaces are known in advance, they can be represented in the digital blueprints of the parts to be modeled. Modern automatic mesh generators such as Gmsh [2] can generate meshes that are conforming to these interfaces. When a physical model involves discontinuous material properties, interfaces can develop/nucleate, grow, change topology or disappear. These interfaces can be material or immaterial, depending on whether the material par-

ticles move with the interface or not. The position and speed of these interfaces is not known in advance and is part of the computation.

In this paper, we study the case of material interfaces between two immiscible fluids which material properties such as viscosity or density are discontinuous. The existence of surface tension adds for the possibility of a pressure jump at the interface between the two fluids. There is an extensive literature on the use of finite elements to simulate two-phase flows [3]. One can classify the approaches in two main categories: interface-tracking and interface-capturing methods.

In the case of interface tracking, the mesh has the duty to track the interface that remains consistently meshed during its movement. The most accurate methods in this category are the ALE methods [4] where the nodes of the mesh are moved with the velocity of the interface. ALE methods have excellent conservation properties [5]. They are accurate and relatively simple to implement, but their biggest drawback is that they do not allow – at least in their pure version – large deformations of the interface or topology changes. Some papers propose to use mesh adaptation in combination with ALE but frequent mesh adaptations have the consequence to introduce time discontinuities in the solution. It is possible to mitigate this issue by only performing few mesh adaptations and use a fixed point algorithm [6]. Nevertheless, these techniques move away from the original simplicity of ALE methods by introducing the complexity and relative fragility of a mesh adaptation in time.

Interface capturing methods generally consider a fixed mesh and an indicator function, discretized on this fixed mesh, which indicates the position of the interface. For example, in level set methods [7], the indicator function is the signed distance to the interface and the iso-zero of this function represents the interface. Interface capturing methods have complementary advantages and disadvantages to interface tracking methods. They allow topology changes but require profound changes in finite element formulations.

It should be noted that there are sharp and diffuse versions of interface tracking and capturing methods. Diffuse methods consist in regularizing the physical properties of the two fluids, i.e. in smoothing the viscosities and densities of the two fluids over a ϵ thickness. It can be shown that the error committed by diffusing the physical properties

is of the order of $\sqrt{\epsilon}$ [8] which means that diffuse methods can only be accurate if the mesh is refined – possibly anisotropically – in the vicinity of the interface.

Recently, we developed a tracking method called X-Mesh that had the following specifications: i) to be sharp, ii) to work on a fixed topology mesh and iii) to allow large topological changes of the interfaces. The first X-Mesh paper was dealing with the immaterial interface computation of phase-changes using the Stefan model [9]. This paper aims to develop X-Mesh in the context of material interfaces and in particular to solve two-phase flow problems.

2. Governing Equation

We consider the flow of two immiscible, incompressible and Newtonian fluids interacting together via an interface Γ . The evolution of the velocity and pressure of each fluid in time is described by the incompressible Navier-Stokes equations:

$$\begin{aligned}\rho(\partial_t \mathbf{u} + \mathbf{u} \cdot \nabla \mathbf{u}) &= -\nabla p + \mu \nabla^2 \mathbf{u} + \mathbf{f} \\ \nabla \cdot \mathbf{u} &= 0\end{aligned}\tag{1}$$

where \mathbf{u} is the velocity field $(u, v)^T$, p is the pressure, ρ is the density, \mathbf{f} the forces at distance (gravity) and μ the dynamic viscosity.

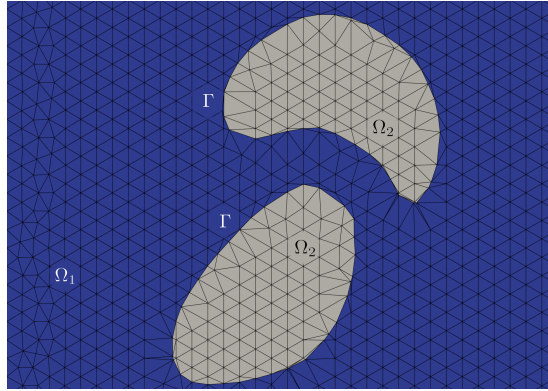


Figure 1: Two-phase flow sketch.

The two fluid phases are noted Ω_1 and Ω_2 (see Figure 1) and have different dynamic viscosity and density (ρ_1, μ_1) and (ρ_2, μ_2) , respectively. These material properties are thus discontinuous across the interface Γ . The Navier-Stokes equations are solved simultaneously on both subdomains and boundary conditions at the interface are necessary. The two equations 1 correspond to the conservation of momentum and the conservation of mass. These conservation laws must be respected at the interface between the two fluids. The conservation of mass leads to the condition of continuous velocity in the normal direction at the interface, thus preventing the transfer of mass between the two phases:

$$[\mathbf{u}] \cdot \mathbf{n} = 0$$

where the brackets $[\cdot]$ refer to the jump at the interface.

In addition to the condition of impermeability of the interface, the conservation of the momentum in the perpendicular direction to the interface must be respected. To satisfy this condition, the jump in normal stress is counterbalanced by the surface tension

$$\left[-pI + \mu \frac{1}{2} (\nabla \mathbf{u} + \nabla \mathbf{u}^T) \right] \cdot \mathbf{n} = \sigma \kappa \mathbf{n} \quad (2)$$

with I the identity operator, σ the surface tension coefficient and κ the curvature of the interface.

In two-phase flows, the main challenge is to compute the position of the interface accurately. When we talk about accuracy, we mean two things. We must be able to compute complex mobile interfaces whose topology changes but we should ideally compute an interface whose position is such that the mass of each of the two fluids is conserved. In this first X-Mesh multi-phase paper, we will show that it is possible to track very complex fronts with topology changes using a mesh with a fixed connectivity. To describe the position of the interface, we use here a classical technique. An indicator function $\phi(x, y)$ is discretized on the same mesh as the one used to discretize the fluid pressure and velocity. This *level set* function [10] classically represents the signed distance to Γ . Thus, in the standard setting, the evolution in time of the level set function ϕ and therefore of the interface is governed by the advection equation:

$$\partial_t \phi + \mathbf{u} \cdot \nabla \phi = 0 \quad (3)$$

with \mathbf{u} corresponding to the velocity of the fluids obtained in equations 1.

3. Finite Element Solver

In this section we describe our numerical method for the resolution of two-phase flows. We choose to work with the finite element method and more specifically with the Galerkin approach and stabilized P1 elements for solving both the level set equation 3 and the Navier-Stokes equations 1. The algorithm to deform the mesh in order to follow the interface is then explained in section 3.3. Finally, a sequential coupling between these steps is presented.

3.1. Navier-Stokes solver

The different flows targeted by our approach can be dominated by advection, the continuous Galerkin finite element method must then be stabilized to avoid spurious oscillations. Several stabilizations have been developed for this purpose. In this work, we use the Streamline Upwind/Petrov-Galerkin (SUPG) method [11]. In order to minimize the size of the linear system to solve, our unknowns are positioned at the nodes of our mesh. However, this does not respect the Babuska-Brezzi condition [12] and leads to the appearance of high frequencies in the pressure field. We get around this problem by using the popular Pressure-Stabilizing/Petrov-Galerkin (PSPG) stabilization [13].

In our X-Mesh approach, we use a mesh that has a fixed connectivity: only vertex positions change with time. Coordinates of the mesh vertices are thus a variable denoted $\mathbf{x}(t)$. The mesh moves to permanently match the interface, this displacement is taken into account via a non-conservative ALE formulation consisting in removing the mesh velocity \mathbf{w} in the advection term. The time is discretized using a constant time step Δt . We denote discrete time instants of variables that depend on time – mesh positions $\mathbf{x}(t)$ for example – as $\mathbf{x}_n = \mathbf{x}(n\Delta t)$. The mesh velocity is thus $\mathbf{w} = (\mathbf{x}_{n+1} - \mathbf{x}_n)/\Delta t$. For the temporal integration we use the implicit Euler scheme and we obtain the discrete formulation with the finite element method.

Consider $\mathbf{S}_\mathbf{u}$ and \mathbf{S}_p , the solution spaces of \mathbf{u}_{n+1} and p_{n+1} , respectively and their test functions $(\mathbf{v}_{n+1}, q_{n+1}) \in \mathbf{V}_\mathbf{u} \times \mathbf{V}_p$.

The fully discrete formulation of (1) is to find $(\mathbf{u}_{n+1}, p_{n+1}) \in \mathbf{S}_u \times \mathbf{S}_p$ such that for any $(\mathbf{v}_{n+1}, q_{n+1}) \in \mathbf{V}_u \times \mathbf{V}_p$:

$$\begin{aligned} & \int_{\Omega} \rho \left((\mathbf{u}_{n+1} - \mathbf{u}_n) \frac{1}{\Delta t} + (\mathbf{u}_{n+1} - \mathbf{w}) \cdot \nabla \mathbf{u}_{n+1} \right) \cdot \mathbf{v}_{n+1} d\Omega \\ & + \int_{\Omega} \mu \nabla \mathbf{u}_{n+1} : \nabla \mathbf{v}_{n+1} d\Omega - \int_{\Omega} \nabla p_{n+1} \cdot \mathbf{v}_{n+1} d\Omega = \int_{\Omega} \rho \mathbf{g}_{n+1} \cdot \mathbf{v}_{n+1} d\Omega + \text{SUPG} \quad (4) \\ & \int_{\Omega} \nabla \cdot \mathbf{u}_{n+1} q_{n+1} d\Omega + \text{PSPG} = 0 \end{aligned}$$

With SUPG the term for the SUPG stabilization and PSPG the term from the PSPG stabilization that can be expressed in function of the residual \mathcal{R} of the equation:

$$\begin{aligned} \text{SUPG} &= \int_{\Omega} \tau_{\text{SUPG}} \mathcal{R}_{n+1} (\mathbf{u}_{n+1} - \mathbf{w}_{n+1}) \cdot \nabla \mathbf{v}_{n+1} d\Omega \\ \text{PSPG} &= \int_{\Omega} \tau_{\text{PSPG}} \nabla q_{n+1} \mathcal{R}_{n+1} d\Omega \\ \mathcal{R}_{n+1} &= \left(\rho (\mathbf{u}_{n+1} - \mathbf{u}_n) \frac{1}{\Delta t} + \rho ((\mathbf{u}_{n+1} - \mathbf{w}) \cdot \nabla \mathbf{u}_{n+1}) - \nabla p_{n+1} - \rho \mathbf{g}_{n+1} \right) \end{aligned}$$

with τ_{SUPG} and τ_{PSPG} the coefficient for the SUPG and PSPG stabilisation respectively.

The classical finite element spatial discretization yields a nonlinear system of equations for \mathbf{u}_{n+1} and p_{n+1} that can be solved using a Newton scheme. For the Navier-Stokes solver we used the open-source software Migflow [14].

3.2. Level set solver

The position of the interface between the two fluids is described by the iso-contour $\phi = 0$ of the level set function and its temporal evolution is determined by the advection equation 3. As for the resolution of the Navier-Stokes equations, we stabilize the advection via an SUPG term [11]. The resolution of the equation is done on a fixed mesh, we thus drop the index notation for the computational domain Ω and the time integration is solved by a Crank Nicolson method. Let \mathbf{S}_{ϕ} be the solution space of ϕ_{n+1} and $w_{n+1} \in \mathbf{V}_{\phi}$ be the test function associated to ϕ_{n+1} . The discrete formulation can then be written as follows:

Find $\phi_{n+1} \in \mathbf{S}_\phi$ such that for any $\psi \in \mathbf{V}_\phi$:

$$\begin{aligned} & \int_{\Omega} (\phi_{n+1} \psi - \phi_n \psi) \frac{1}{\Delta t} d\Omega + \frac{1}{2} \int_{\Omega} (\mathbf{u} \cdot \nabla \phi_n \psi + \phi_n \nabla \cdot \mathbf{u} \psi) d\Omega \\ & + \frac{1}{2} \int_{\Omega} (\mathbf{u} \cdot \nabla \phi_{n+1} \psi + \phi_{n+1} \nabla \cdot \mathbf{u} \psi) d\Omega + \text{SUPG} = 0 \end{aligned}$$

The SUPG stabilisation term depends of the residual of the advection equation and is given by:

$$\begin{aligned} \text{SUPG} &= \int_{\Omega} \tau_{\text{SUPG}} \mathbf{u} \cdot \nabla \psi \mathcal{R} d\Omega \\ \mathcal{R} &= \left((\phi_{n+1} - \phi_n) \frac{1}{\Delta t} + \frac{1}{2} (\mathbf{u} \cdot \nabla \phi_n + \phi_n \nabla \cdot \mathbf{u}) + \frac{1}{2} (\mathbf{u} \cdot \nabla \phi_{n+1} + \phi_{n+1} \nabla \cdot \mathbf{u}) \right) \psi \end{aligned}$$

The finite element method then allows us to spatially discretize the domain and we obtain a system of linear equations. Since we don't take into account the mesh displacement in the resolution of the advection equation, after moving the mesh with the deforming algorithm presented in the following section the value of the level set at the nodes aren't correct. To compute the new values at the nodes of the level set we use a fast-marching algorithm [15] that computes an approximate signed distance to the front. Since the interface is completely embedded by the edges of the mesh, the seeds of the algorithm from which the level set value propagates in the mesh are the front nodes showed in Figure 4 (f).

3.3. Extreme mesh deformation – Front relaying

The idea behind the X-Mesh method [9] is to deform a mesh with continuous node movements to constantly match the interfaces of interest, even in the case of topological changes of the fluids domains. The mesh however keeps a fixed topology. To achieve this goal, the method allows elements to become degenerated, meaning that a triangle can deform down to an edge or even a point. This enables the mesh to deform continuously in time and ensure the relay of the front. The interface is transferred from one node to another located at the same position allowing the interface to propagate like a baton in a relay race.

There are two ways for a triangle to degenerate into an edge. In the first case, one of the three edges of the triangle collapses to a single point so the opposite angle to this

edge degenerates to 0 radians. Such an element is called *a needle*. In the second case, one of the three vertices of the triangle tends to a point that belongs to its opposite edge so the angle associated with this node tends to π radians. Such an element is called *a cap*.

The use of degenerate or quasi-degenerate elements leads to two specific difficulties: *conditioning and stability*.

3.3.1. Conditioning

The first problem that appears with the use of degenerate or quasi-degenerate elements is the bad conditioning of the finite element matrices. Assume a triangle with 3 vertices i , j and k and with internal angles θ_i , θ_j and θ_k (see Figure 2).

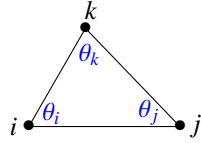


Figure 2: A triangle with its three internal angles θ_i , θ_j and θ_k .

The local stiffness matrix $[K]$ that corresponds to the discretization of the $-\nabla^2$ operator can be written in its cotangent form as

$$[K] = \begin{bmatrix} \cot(\theta_j) + \cot(\theta_k) & -\cot(\theta_k) & -\cot(\theta_j) \\ -\cot(\theta_k) & \cot(\theta_i) + \cot(\theta_k) & -\cot(\theta_i) \\ -\cot(\theta_k) & -\cot(\theta_i) & \cot(\theta_i) + \cot(\theta_j) \end{bmatrix}$$

Whether we are talking about a needle or an cap, at least one of the angles $\theta_{i,j,k}$ of a degenerate triangle will tend to zero which implies that the cotangent of this angle will tend to infinity. More precisely, the stiffness matrix $[K]$ necessarily contains a zero eigenvalue $\lambda_1 = 0$ which corresponds to the rigid body or constant mode $v_1 = (1, 1, 1)$. When this element is degenerated, another eigenvalue λ_2 also tends to zero and the third one, λ_3 tends to infinity.

Let us imagine the case of a needle: vertex i and vertex k eventually coincide. The mode that correspond to zero eigenvalue λ_2 is $v_2 = (1, 0, -1)$. Mode v_2 is the only mode besides v_1 – the rigid body mode – that can exist in the finite element solution because any other combination that involves v_3 leads to an infinite energy. Thus, at the zero measure limit, the finite element solution is such that the nodal values of the unknown at nodes i and k are the same.

Now let's build a cap: vertex k moves at position

$$\mathbf{x}_k = \mathbf{x}_i\alpha + \mathbf{x}_j(1 - \alpha) \quad , \quad \alpha \in]0, 1[.$$

The mode that correspond to zero eigenvalue λ_2 is $v_2 = (\alpha, 1 - \alpha, -1)$ which implies that in the zero measure limit, the finite element solution will be linear along the straight line ikj .

Why was the difference made between a needle and a cap? In both cases, the global stiffness matrix will suffer from poor conditioning but linear solvers – even iterative ones – behave very well in the case of very large eigenvalues. Any preconditioner will solve this problem. In this paper, we proceed in the same fashion as in [9]. We simply limit the maximum value of λ_3 by limiting the minimum value of the area of degenerated triangles. In future work, we will propose robust preconditioners for X-Mesh. The difference between a needle and a cap is in the stability as we will detail below. A needle imposes a local constraint between two degrees of freedom while a cap couples the three degrees of freedom of the triangle.

3.3.2. Stability

If stability is lost, then the convergence of the finite element method is lost as well. Historically, the finite element community took from the seminal paper of Babuška and Aziz [16] that, to ensure finite element convergence, it was sufficient to generate meshes whose triangles did not have very obtuse angles. Stability issues are thus essentially related to the presence of caps in the mesh. Many have considered that this *angle condition* was a necessary condition for the convergence of finite elements, but this is not correct: it is a sufficient condition – Babuška and Aziz have never said the contrary. The angle condition can be significantly weakened [17]. An isolated cap in a mesh will not cause any stability concerns. It is only when caps are joined together in long bands that stability problems arise. If usual P1 triangles are used, it is easy to show that a band of n caps of individual length h ($h = \|\mathbf{x}_j - \mathbf{x}_i\|$ in Figure 2) prevents non-linear variations of the solution along the whole band length nh (locking) and thus degrades the convergence from h^2 to $(nh)^2$. On the other hand, as we have shown above, needles impose local constraints on the solution and these constraints therefore do not prop-

agate to great distances. We can therefore have as many needles as we want without worrying about stability.

Our mesh deformation/relaying algorithm has from the beginning taken into account this constraint of not creating bands of caps. Assume a triangular mesh that exactly represent a front at a given time t (Top-left image of Figure 3). The front moves to the right of a constant speed v during a time Δt and thus we can move front vertices to the right of $v\Delta t$ (Top-center image of Figure 3) and then of $v\Delta t$ again (Top-right image of Figure 3). At that point, one sees that the relay will essentially occur with triangles that have the form of a cap and that caps are arranged in bands. Such an algorithm clearly leads to stability problems and should be avoided. In general, if we are not careful, a mesh deformation algorithm will naturally tend to create these bands of caps.

What if now mesh vertices move along edges of the current mesh (Bottom images of Figure 3). Then, a majority of needles will be created. Isolated caps may be created but their number only depends on the difference between the number of vertices upstream and downstream the front. Another ingredient of the algorithm is to move the vertices only upstream of the front. This allows the relay process to run smoothly, without having downstream vertices moving in the opposite direction of the front movement and creating some kind of *traffic jam* [9]. Finally, when a vertex of the front has passed the relay to another vertex, it progressively returns to its initial position which allows to maintain a quality mesh upstream of the front.

3.3.3. Front relaying

Figure 4 shows the algorithm used to deform the mesh between 2 time steps so that it continuously conforms to the new interface. This interface is defined by $\phi = 0$ and the sign of ϕ determines the phase of the fluid. On images (a) and (b) of Figure 4, the phases of the fluids for 2 consecutive time steps t and $t + \Delta t$ are represented in blue and grey. The idea of X-Mesh is that the mesh at the two times t and $t + \Delta t$ must conform to the interface. Image (b) shows the phases at time $t + \Delta t$ on the mesh at time t . The new interface at time $t + \Delta t$ – in dashed lines – is not conforming to the mesh.

The objective of the front relaying algorithm is to deform the existing mesh at time t

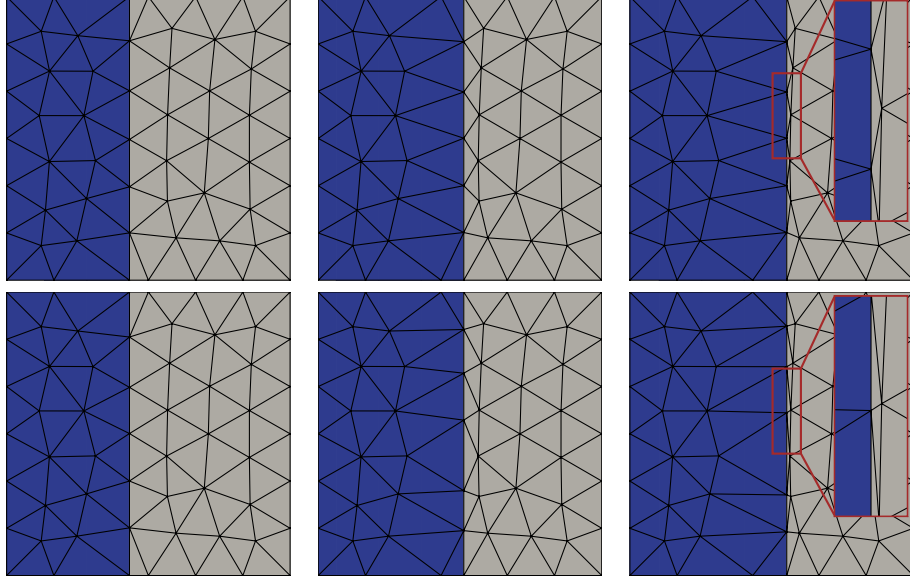


Figure 3: Moving the nodes along their velocity (top) or along the edges (bottom).

so that the mesh is conformal to the new interface: we want the interface at time $t + \Delta t$ to be entirely represented by the edges of the mesh. Additionally, the algorithm must limit as much as possible the creation of bands of caps for stability reasons. As mentioned above, moving the vertices along the edges of the mesh allows to avoid the creation of bands of caps. We also want to avoid vertices to accumulate downstream the front. Thus, only nodes upstream of the front should move towards the front. This starting point allows us to develop a robust front relaying algorithm. The region in green of image (c) of Figure 4 represent the region where phases have changed between t and $t + \Delta t$. This region is thus upstream of the front and vertices that move should be chosen in this region. We call *active vertices* the vertices for which the sign of the level set ϕ has changed during the time step. Active vertices include vertices of the previous front which had a level set value of 0 and are coloured in yellow in image (c) of Figure 4.

An edge (ij) is a cut-edge if, at time step t , its two nodes have a different sign for the level set ϕ at time $t + \Delta t$. There is therefore a potential target on the cut-edge (ij) where the level set is null, i.e. where the new front will be located at $t + \Delta t$. All active vertices that belong to cut-edges will move: we call them moving vertices (see image (d) of

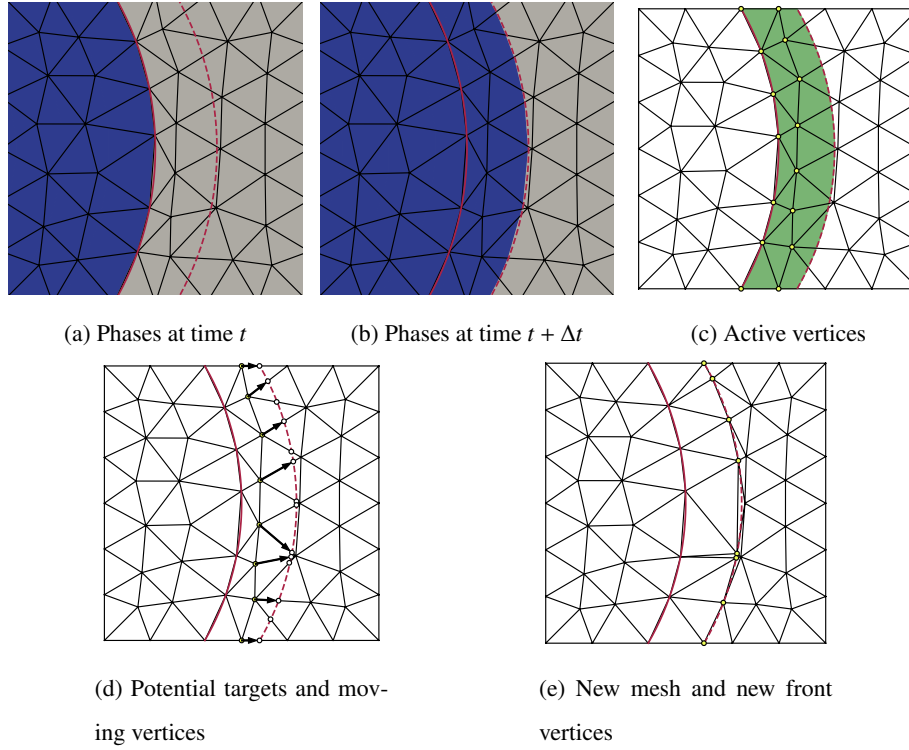


Figure 4: Mesh deformation algorithm.

Figure 4). Now a moving vertex can belong to more than one cut-edges so we have to choose one of the potential targets. Experimentally, we found that using the potential target that corresponds to the smallest vertex displacement allowed to generate more regular meshes. An exception to this rule concerns the vertices of the boundary, which obviously move along the boundary. Image (d) of Figure 4) show moving vertices and their trajectories to their final targets. Image (e) of Figure 4) shows mesh at time $t + \Delta t$ that is conforming to the new interface.

A last ingredient of the front relaying algorithm is to progressively move vertices that have left the front to their original position. This feature allows to restore a nice mesh upstream the front when the front has passed.

3.4. Coupling

This section describes the algorithm used to couple the different parts presented previously: the resolution of the Navier-Stokes equations, the resolution of the advection equations, the displacement of the mesh with the algorithm proposed for X-Mesh and the redistancing of the level set. All the results of this paper have been obtained with a sequential algorithm presented in Algorithm 1. The simulation of a time step consists in the successive resolution of these different steps. The Navier-Stokes equations are solved to obtain the new velocity field. This velocity field allows us to advect the level set in order to obtain the new level set values on the mesh defined by the positions \mathbf{x}_n . The mesh is then deformed to match the new interface defined by the level set. Since the mesh has moved, the level set values at the nodes are no longer correct. We then obtain the new level set for the new positions of the mesh \mathbf{x}_{n+1} by applying the fast-marching method [15] with the nodes of the front in $n + 1$ as seeds. This coupling has shown a very good robustness in practice for test cases with many topological changes. To increase the accuracy of the scheme, one could be tempted to iterate between the mesh deformation and the solution of the Navier-Stokes equations. This would allow the mesh deformation between t_n and t_{n+1} to be taken into account directly in the equations between t_n and t_{n+1} . This is however not trivial and a simple fixed point method does not converge quickly. The position of the mesh can oscillate between two states without converging, especially when there is a sudden change of configuration e.g. when a topological change occurs.

Algorithm 1 Sequential coupling for one time-step

$\mathbf{u}_{mesh} = (\mathbf{x}_n - \mathbf{x}_{n-1}) \frac{1}{\Delta t}$
 $\mathbf{u}_{n+1} = \text{Navier-Stokes}(\mathbf{u}_n, \phi_n, \mathbf{u}_{mesh})$
 $\phi_{adv} = \text{level set}(\mathbf{u}_{n+1}, \phi_n)$
 $\mathbf{x}_{n+1}, \text{front}_{n+1} = \text{X-Mesh}(\mathbf{x}_n, \phi_{adv}, \phi_n, \text{front}_n)$
 $\phi_{n+1} = \text{Fastmarching}(\mathbf{x}_{n+1}, \text{front}_{n+1})$
 $t = t + \Delta t$

4. Surface Tension

When considering a two-phase flow, depending on the material properties of the two fluids and the problem considered, it is not always possible to neglect surface tension. This is notably the case for a large number of industrial processes where flows related to the dynamics of bubbles appear. A good representation of the surface tension is essential to correctly simulate these flows. From equation 2 we can directly link the surface tension to the conservation of momentum condition at the interface. Indeed, when this condition is taken in the direction normal to the interface, it is expressed by:

$$\begin{aligned} \mathbf{n} \cdot \left[-p\mathbf{I} + \mu \frac{1}{2} (\nabla \mathbf{u} + \nabla \mathbf{u}^T) \right] \cdot \mathbf{n} &= \mathbf{n} \cdot \sigma \kappa \mathbf{n} \\ [p] &= -\sigma \kappa + \mathbf{n} \cdot \left[\mu \frac{1}{2} (\nabla \mathbf{u} + \nabla \mathbf{u}^T) \right] \cdot \mathbf{n} \\ [p] &= -\sigma \kappa \end{aligned} \quad (5)$$

The term $\mathbf{n} \cdot \left[\mu \frac{1}{2} (\nabla \mathbf{u} + \nabla \mathbf{u}^T) \right] \cdot \mathbf{n}$ is exactly 0 because both fluids are considered Newtonian and incompressible. It is therefore possible to obtain the value of the pressure drop at the interface based on the curvature of the interface and the surface tension coefficient. In the ghost fluid method, the surface tension is modeled by imposing this pressure jump at the interface. On fixed mesh, the pressure gradient operator ∇p is modified to take into account the classical pressure in addition to the pressure jump for the elements intercepted by the interface. One could then think that the method is sharp because the pressure jump is well located at the interface however the interface has a thickness of the size of an element. Indeed, the method is insensitive to a displacement of the interface of $\pm \frac{h}{2}$ with h the element size [18]. In our approach we also use the pressure jump to model the surface tension effects. The main difference with the ghost fluid method is that the nodes of our mesh are positioned exactly on the interface, so we have to impose the pressure jump on the node. The modified pressure \bar{p} used in the ∇p operator of equation 4 is only different for the boundary nodes which will have as value:

$$\bar{p}_i = \begin{cases} p_i & \text{if } \Omega_e \in \Omega_1 \\ p_i + \sigma \kappa_i & \text{if } \Omega_e \in \Omega_2 \end{cases}$$

with p_i the pressure at node i , κ_i the interface curvature at node i and Ω_e the considered element.

The representation of the surface tension thus obtained is exactly sharp because contrary to the ghost fluid method on fixed mesh the thickness of the interface is zero. An arbitrarily small displacement of the interface induces a displacement of the mesh which modifies the pressure gradient operator and thus the surface tension.

This pressure jump can be observed in Figure 5 in the case of a static bubble with the classical pressure (a) and the modified pressure (b) which is well constant everywhere except exactly at the interface. When trying to model the surface tension, a very important step is the measurement of the curvature of the interface. As we know the nodes positioned on the interface, it is possible to approximate the curvature by calculating the radius of the circumscribed circle of 3 consecutive nodes belonging to the interface. This very local method has the merit of being exact for the circle, the equilibrium state of the static bubbles. Figure 5 shows the pressure, the modified pressure and the velocity field for the static Laplace bubble. In this validation, a circular bubble without gravity is simulated. The expected pressure inside the bubble was calculated analytically by Laplace and is worth:

$$p_{bubble} = \frac{\sigma}{R}$$

with R the radius of the bubble. This expression consider that the pressure outside the bubble is zero.

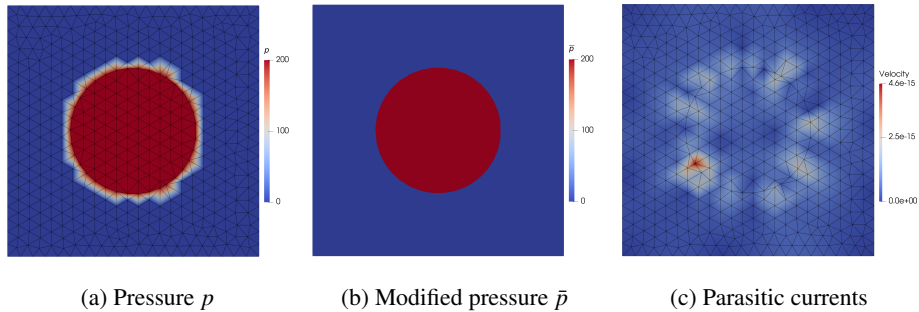


Figure 5: Static bubble.

The bubble is supposed to remain completely stationary and the velocity field should therefore be exactly 0 but due to numerical inaccuracies or poor numerical modeling of the surface tension, spurious currents may appear. In figure 5 c, we can observe the parasitic currents obtained for the approach presented in this article. These have a norm of 10^{-15} and are therefore of the order of machine precision. The continuous pressure p and the modified (discontinuous) pressure \bar{p} is also represented in the two first figure of 5. In this case the bubble considered has a radius of size $R = 0.5 [m]$ and the surface tension considered is $\sigma = 100 [N/m]$. The obtained pressure inside the bubble is $p = 200 [Pa]$ as expected by the Laplace formula. The time t_{obs} at which the pressure and the velocity field is observed is 250 times greater than the characteristic time of this problem $t_{char} = \frac{D\mu}{\sigma}$.

5. Results

In this section we test our method by applying it on a validation case for a sloshing problem. Several test cases are then used to compare our method to different reference results.

5.1. Verification of the solver – sloshing

The *sloshing problem* consists in computing the free oscillations of a liquid in a tank. This problem essentially allows to verify that our solver solves the right equation because it is one of the few cases where an analytical solution exists in the case of small perturbations of a planar interface [19]. In the analytical setting, the interface is sufficiently simple so that it can be represented by a height function $\eta(x, t)$ that is initialized as

$$\eta(x, 0) = d + \eta_0 \sin k (0.5 - x)$$

where $d = 0.5$ is the mean elevation, $\eta_0 = 0.01$ is the initial oscillation amplitude and k is the wave number.

The analytical evolution of the maximum height of the free surface η depend on $\nu = \frac{\mu}{\rho}$ the kinematic viscosity and the dimensionless parameter $\kappa = \frac{g}{\nu^2 k^3}$:

$$\frac{\eta(t)}{\eta_0} = 1 - \kappa e^{-\nu k^2 t} f(\nu k^2 t)$$

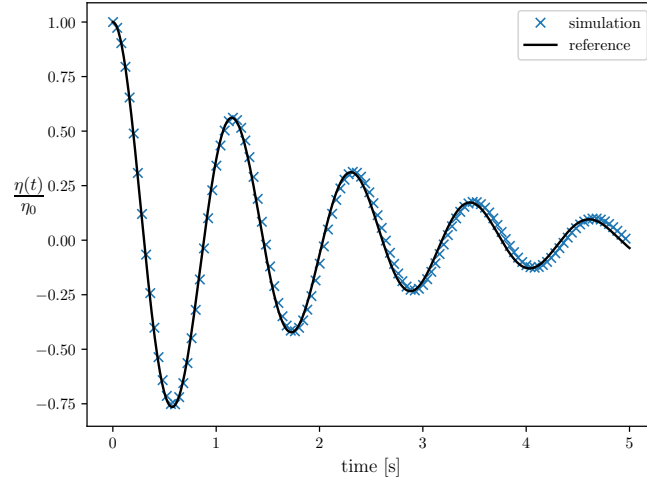


Figure 6: Wave elevation evolution in a sloshing problem.

where $f(t)$ is the inverse Laplace transform of the function

$$F(s) = \frac{1}{(s-1)((s+1)^2 - 4s^{\frac{1}{2}} + \kappa)}.$$

The computational domain considered is a rectangle of dimensions $[0, d] \times [0, 1.3d]$ and the four wall have free slip condition.

Figure 6 shows the evolution of the perturbation η over time. We can observe that the simulation is in good agreement with the analytical solution. Since this analytical solution is obtained from the linearized Navier-Stokes equations, the initial perturbation $\eta_0 = 10^{-2}$ cannot be too large with respect to $d = 0.5$.

For the reference solution of the linearized Navier-Stokes equations to be valid, the amplitude of the sloshing must be small enough. However, the mesh used for this simulation is quite coarse with 3900 vertices. At the beginning of the simulation the characteristic size of the elements is smaller than the amplitude of the sloshing and thus a relay of the front is done between the different vertices. However, quite quickly the amplitude of the sloshing decreases and the simulation is close to a classical ALE simulation without relaying of the interface

5.2. Dambreak

The dambreak test case consists of the collapse of a fluid water column in a container. It corresponds to the sudden rupture of a dam and the flow of the impounded water. The evolution of the interface in this problem is complex and involves multiple topology changes. Its complexity has made it a reference test case to validate two-phase flow simulations. The considered column has height $H = 0.4 [m]$ and width $L = 0.4 [m]$. It collapses in a calculation domain of size $1.4 \times 1.1 [m^2]$. Boundary conditions of free-slip are applied to the 4 walls. The mesh used has 75,950 vertices. Figure 7 represents the evolution of the free surface at the different adimensional times $t = 0.5, 1.75, 3, 5.5, 6.5$ and 22.5 , where the reference time considered is $t_{ref} = \sqrt{h/g}$. Despite the numerous topological changes present during a dambreak, the method is robust enough to simulate such complex flows.

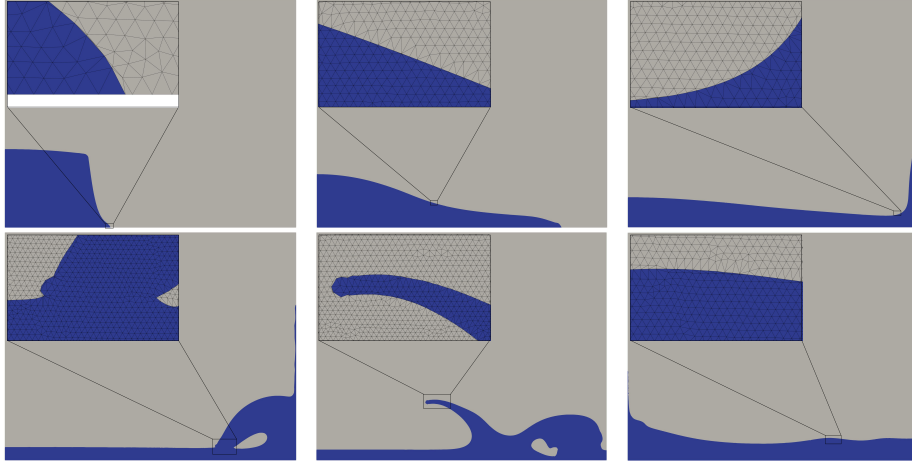


Figure 7: Dambreak simulation: Free surface position for the adimensional times $t = 0.5, 1.75, 3, 5.5, 6.5$ and 22.5 .

5.3. Rayleigh-Taylor

Rayleigh-Taylor instability consist in placing a heavier fluid above a lighter one. This position is an unstable equilibrium and is sensible to any perturbation. A classical benchmark for the validation of two-phase flows solver is to trigger a single-mode

perturbation in the initialisation. The instability develops under the influence of the gravity field and is commonly occurring in a wide range of physical phenomena. A disturbance is initialized in the interface position at $t = 0$ and it's initial position is given by:

$$y = 2.0 + 0.05 \cos 2\pi x$$

Initially, the velocity field is set to 0 and the pressure is hydrostatic. The evolution in time of the 2 fluids is determined by 2 adimensional numbers, the Atwood (At) and Reynolds (Re) numbers defined in our case by:

$$At = \frac{\rho_1 - \rho_2}{\rho_1 + \rho_2}$$

$$Re = \frac{\sqrt{WgW}}{\nu}$$

with W the width of the canal.

Figure 8 (top) shows the evolution of the two phases for the case $At = 0.5$ and $Re = 256$. Our results are in good agreement with those of He et al. [20] for a mesh of approximately 262,000 elements with the lattice boltzmann method. The sharp interface of the presented method as well as the fine mesh used (about 123,000 vertices) allows to keep features of the flow for a long time. The flow becomes asymmetric around $t = 8.75$ when the filament thickness becomes smaller than the characteristic size of the mesh elements. The flow can no longer be properly captured because the level set will have elements with triple zero value. The phase of the filament is not represented anymore and a mass loss is observed. This loss depends on the mesh size and since the mesh is asymmetric, the flow becomes asymmetric too. The impact of the characteristic length of the mesh is shown at Figure 8 (bottom) where the same Rayleigh-Taylor instability was simulated but with a 4 times coarser mesh (about 31,000 vertices). The small features of the flow disappears quicker with the coarser mesh as expected. An analytical solution for the linearized equations exist and is valid for the linear phase of the instability development [21]:

$$h = h_0 e^{\hat{\alpha} t}$$

with h the perturbation size, h_0 the perturbation at $t = 0$ and $\hat{\alpha}$ the growth rate. For the parameter of the simulation the analytical grow rate is $\hat{\alpha}_a = 9.3$ and the observed one is $\hat{\alpha}_o = 9.2$.

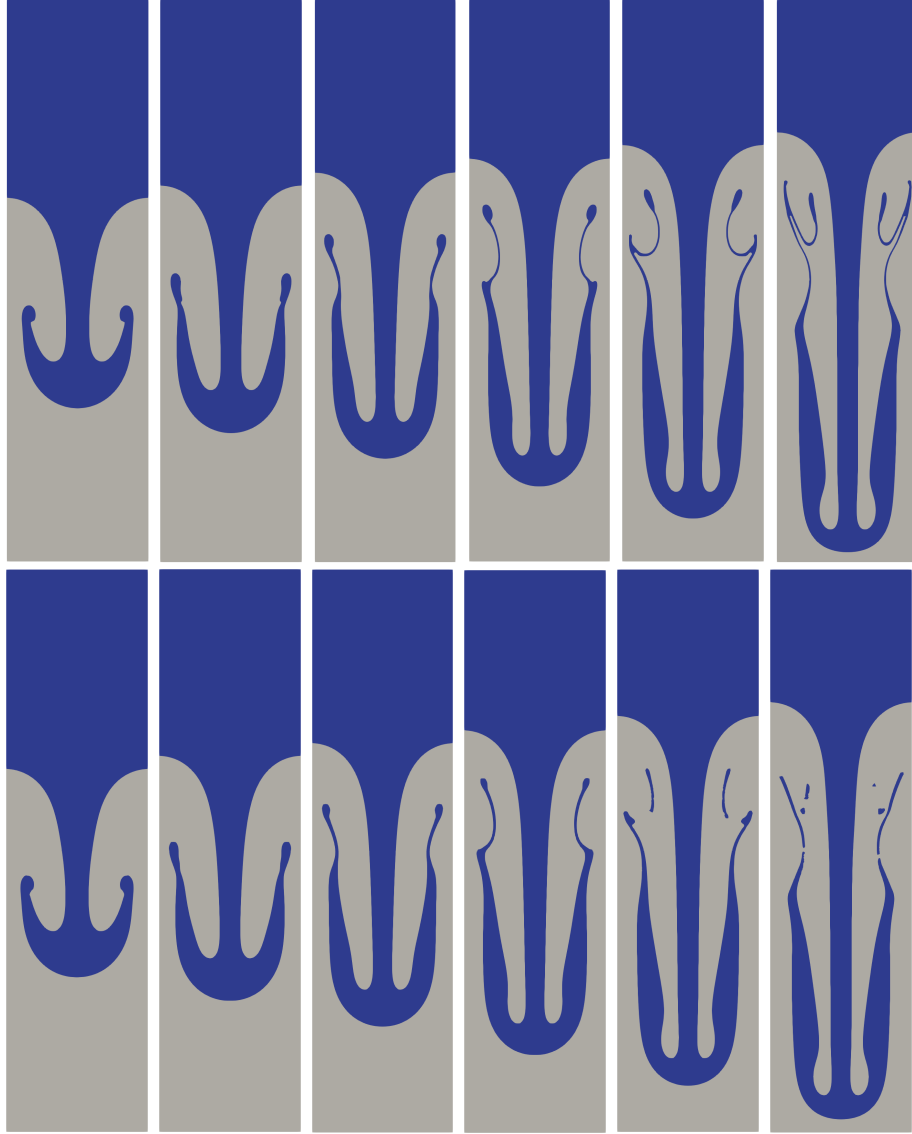


Figure 8: Rayleigh-Taylor instability for $Re = 256$, $At = 0.5$ at times $t = 3, 3.5, 4, 4.5, 5, 5.5$ with a fine mesh (top) and a coarser mesh (bottom).

5.4. Single Bubble rising

Bubble dynamics are frequently encountered in a variety of industrial processes or natural flows. The correct representation of the interface is essential for this type of problem because the surface tension force is proportional to the curvature of the interface. Grace et al [22] have characterized in 1976 the final shape obtained during single bubble rise experiment for different fluids. Figure 10 summarizes their observations. To validate our method for bubble dynamics we try to reproduce theses results. The y axis of Figure 10 correspond to the Reynolds number and it's x axis to the Bond (or Eötvös) number. Theses number can be computed for the case of bubbles by

$$Re = \frac{\rho_1 \sqrt{g} D^{3/2}}{\mu_1}$$

$$Bo = \frac{\rho_1 g D^2}{\sigma}$$

where D is the diameter of the bubble and the subscripts 1 corresponds to the heavier fluid.

We consider three cases with different pairs of Reynolds and Bond numbers represented in Figure 9 and on Grace's diagram at Figure 10. The density and viscosity ratios considered are $\frac{\rho_1}{\rho_2} = 1000$ and $\frac{\mu_1}{\mu_2} = 100$. The diameter of the bubble is fixed to $D = 1 [m]$ and to avoid any impact of the lateral wall on the bubble dynamic the computational domain considered is $W = 6 [m]$ width and $H = 12 [m]$ high. The surface tension is applied explicitly engendering a stability condition on the time step. The time step must verify the condition:

$$\Delta t < \sqrt{\frac{(\rho_1 + \rho_2) h^3}{4\pi\sigma}}$$

where h is the characteristic size of the mesh.

The predicted bubble shape matches the experimental. The shapes obtained with the presented method are also in good agreement with the results of [23].

5.5. Bubble merging

To verify that the approach used for the surface tension works during topological changes of the fluid phases, we are interested in a test case of two bubbles superimposed

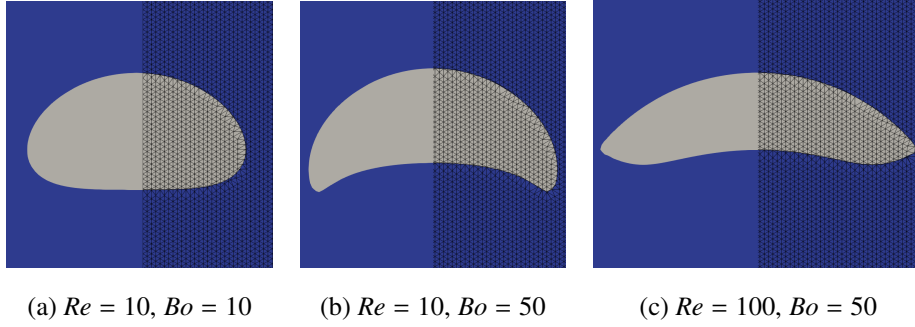


Figure 9: Final form of free rise bubbles

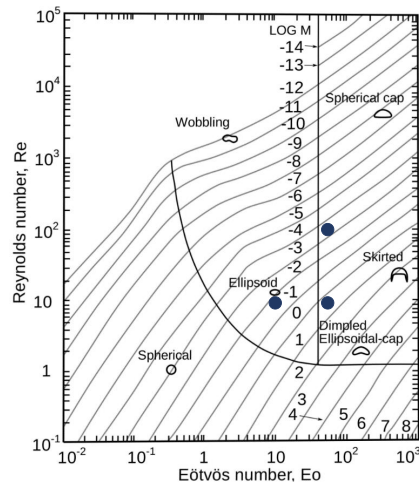


Figure 10: Grace's diagram [22].

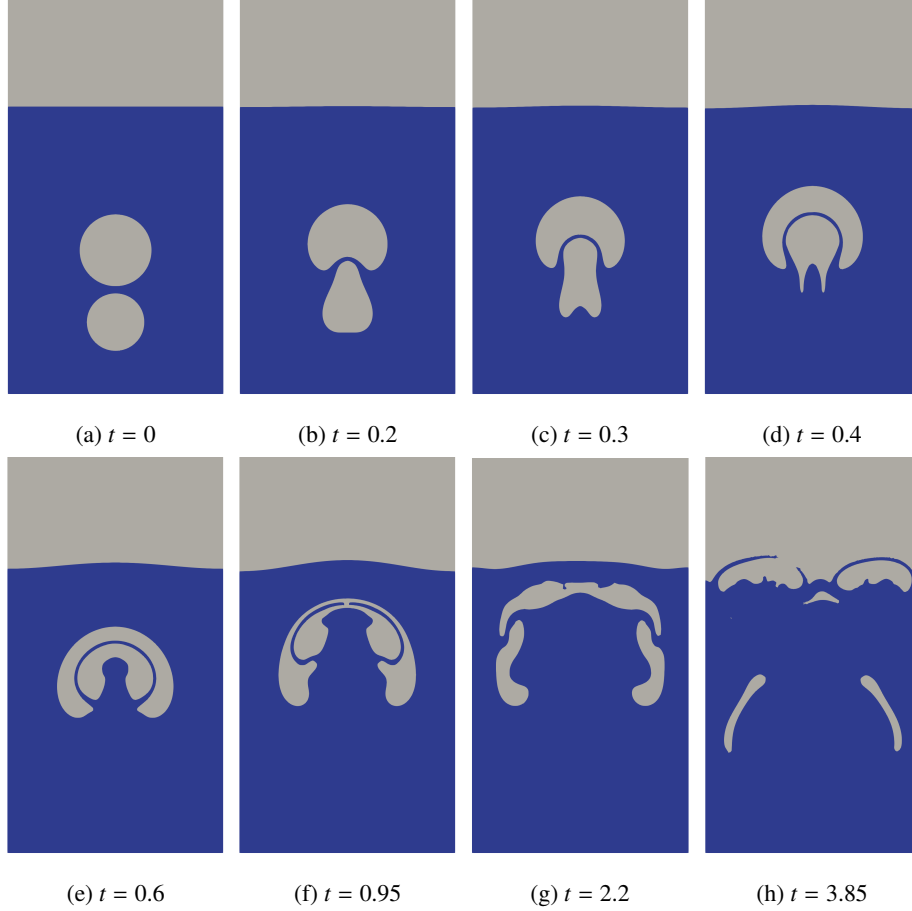
in a column of heavy fluid with a free surface. The computational domain is a 6 by 3 [m] square, the two bubbles are centered horizontally, their center are positionned at height $y = 1$ [m] and $y = 2$ [m] with radius of 0.4 and 0.5 meters respectively. The parameters of the two fluids are chosen such that:

$$\frac{\rho_1}{\rho_0} = 1000 \quad \frac{\mu_1}{\mu_0} = 2 \quad Re = 104 \quad Bo = 313$$

with the Re and Bo numbers defined with the diameter of the greater bubble.

The lower bubble is sucked by the drag of the upper bubble such that at $t = 0.4$ [s]

it is engulfed by the latter. The two bubbles rise together until at $t = 0.95$ [s], the stronger currents in the center of the column push them to collapse. This leads to multiple changes in topology, resulting in two bubbles that rise to the free surface and two elongated bubbles that are carried to the bottom by downward currents on the sides.



6. Conclusion

In this paper we have presented an approach to simulate two-phase flows by modeling the interface in a sharp and low cost way using X-Mesh. The representation of the interface directly in the mesh allows the method to be sharp. It is able to represent discontinuities in the derivatives of velocities at the interface like the ALE methods. The

update of the interface position by means of a level set function allows to easily take into account the changes of the fluid phase topology. The front relay allows the good representation of the large displacements of the interface by carrying out only a local deformation, close to the interface, of the mesh. The presented deformation algorithm allows to keep the original mesh and thus to preserve its topology.

The surface tension model is exactly sharp thanks to the positioning of the nodes on the interface and the imposition of the pressure jump as in the ghost fluid method. Thanks to the calculation of the curvature of the interface via the circumscribed circle of 3 successive nodes, the parasitic currents have been reduced to the order of machine precision. Finally, the sequential algorithm allows to couple the different steps of the simulation in a robust way despite the numerous changes of the fluid phase topology.

However, mass variations have been observed in the simulations. Contrary to what one might think, the variation of the mass is not due to the precision of the advection equation of the level set but to the definition of the level set itself. The level set advection equation is perfectly conservative with respect to the integral of the level set function. However, the mass of the fluid varies because the slope of the level set function does not remain unitary after the advection. For a test case of vortex in a box, where a circular interface is immersed in a vortex velocity field, the level set integral is conserved to the accuracy of the solver. The mass corresponding to the area with a level set value of positive sign varies by an order of 30 %. In future works we intend to remove this level set in order to obtain a mass-conserving method.

Acknowledgements

The authors thank Michel Henry for maintaining the features developed in MigFlow and Nicolas Chevaugeon for his help in implementing the fastmarching algorithm

References

- [1] S. C. Brenner, L. R. Scott, L. R. Scott, The mathematical theory of finite element methods, volume 3, Springer, 2008.
- [2] C. Geuzaine, J.-F. Remacle, Gmsh: A 3-d finite element mesh generator with built-in pre-and post-processing facilities, International journal for numerical methods in engineering 79 (2009) 1309–1331.
- [3] A. Prosperetti, G. Tryggvason, Computational methods for multiphase flow, Cambridge university press, 2009.
- [4] T. J. Hughes, W. K. Liu, T. K. Zimmermann, Lagrangian-eulerian finite element formulation for incompressible viscous flows, Computer methods in applied mechanics and engineering 29 (1981) 329–349.
- [5] M. Lesoinne, C. Farhat, Geometric conservation laws for flow problems with moving boundaries and deformable meshes, and their impact on aeroelastic computations, Computer methods in applied mechanics and engineering 134 (1996) 71–90.
- [6] F. Alauzet, P. L. George, B. Mohammadi, P. Frey, H. Borouchaki, Transient fixed point-based unstructured mesh adaptation, International journal for numerical methods in fluids 43 (2003) 729–745.
- [7] E. Marchandise, P. Geuzaine, N. Chevaugeon, J.-F. Remacle, A stabilized finite element method using a discontinuous level set approach for the computation of bubble dynamics, Journal of Computational Physics 225 (2007) 949–974.
- [8] M. Azaiez, F. Jelassi, M. Mint Brahim, J. Shen, Two-phase stefan problem with smoothed enthalpy, Communications in Mathematical Sciences 14 (2016) 1625–1641.

- [9] N. Moes, J. Remacle, J. Lambrechts, B. Le, The extreme mesh deformation approach (X-MESH) for the stefan phase-change model, *CoRR* abs/2111.04179 (2021).
- [10] J. A. Sethian, P. Smereka, et al., Level set methods for fluid interfaces, *Annual review of fluid mechanics* 35 (2003) 341–372.
- [11] A. N. Brooks, T. J. Hughes, Streamline upwind/petrov-galerkin formulations for convection dominated flows with particular emphasis on the incompressible navier-stokes equations, *Computer methods in applied mechanics and engineering* 32 (1982) 199–259.
- [12] F. Brezzi, On the existence, uniqueness and approximation of saddle-point problems arising from lagrangian multipliers, *Publications mathématiques et informatique de Rennes* (1974) 1–26.
- [13] T. J. Hughes, L. P. Franca, M. Balestra, A new finite element formulation for computational fluid dynamics: V. circumventing the babuška-brezzi condition: A stable petrov-galerkin formulation of the stokes problem accommodating equal-order interpolations, *Computer Methods in Applied Mechanics and Engineering* 59 (1986) 85–99.
- [14] M. Constant, F. Dubois, J. Lambrechts, V. Legat, Implementation of an unresolved stabilised fem–dem model to solve immersed granular flows, *Computational Particle Mechanics* 6 (2019) 213–226.
- [15] J. A. Sethian, A fast marching level set method for monotonically advancing fronts., *Proceedings of the National Academy of Sciences* 93 (1996) 1591–1595.
- [16] I. Babuška, A. K. Aziz, On the angle condition in the finite element method, *SIAM Journal on numerical analysis* 13 (1976) 214–226.
- [17] V. Kučera, On necessary and sufficient conditions for finite element convergence, *arXiv preprint arXiv:1601.02942* (2016).

- [18] S. Popinet, Numerical models of surface tension, *Annual Review of Fluid Mechanics* 50 (2018) 49–75.
- [19] G. Wu, R. Eatock Taylor, D. Greaves, The effect of viscosity on the transient free-surface waves in a two-dimensional tank, *Journal of Engineering Mathematics* 40 (2001) 77–90.
- [20] X. He, S. Chen, R. Zhang, A lattice boltzmann scheme for incompressible multi-phase flow and its application in simulation of rayleigh–taylor instability, *Journal of computational physics* 152 (1999) 642–663.
- [21] P. G. Drazin, W. H. Reid, *Hydrodynamic stability*, Cambridge university press, 2004.
- [22] J. Grace, T. Wairegi, T. Nguyen, Shapes and velocities of single drops and bubbles moving freely through immiscible liquids, *Trans Inst Chem Eng* 54 (1976) 167–173.
- [23] J. Hua, J. Lou, Numerical simulation of bubble rising in viscous liquid, *Journal of Computational Physics* 222 (2007) 769–795.